APL Photonics

Multimode fiber ruler for detecting nanometric displacements

Cite as: APL Photonics **7**, 086103 (2022); https://doi.org/10.1063/5.0089159
Submitted: 23 February 2022 • Accepted: 03 July 2022 • Published Online: 26 August 2022

Ksenia Abrashitova and Lyubov V. Amitonova

ARTICLES YOU MAY BE INTERESTED IN

Target imaging in scattering media using ghost imaging optical coherence tomography
APL Photonics **7**, 086104 (2022); https://doi.org/10.1063/5.0099638

Single-shot all-digital approach for measuring the orbital angular momentum spectrum of light
APL Photonics **7**, 086105 (2022); https://doi.org/10.1063/5.0086536

Epi-fluorescence imaging of the human brain through a multimode fiber
APL Photonics **7**, 071301 (2022); https://doi.org/10.1063/5.0080672

APL Photonics ARTICLE scitation.org/journal/app

Multimode fiber ruler for detecting nanometric displacements

Cite as: APL Photon. 7, 086103 (2022); doi: 10.1063/5.0089159
Submitted: 23 February 2022 • Accepted: 3 July 2022 •
Published Online: 26 August 2022

Ksenia Abrashitova[1] and Lyubov V. Amitonova[1,2,a)]

AFFILIATIONS

[1] Advanced Research Center for Nanolithography (ARCNL), Science Park 106, 1098 XG Amsterdam, The Netherlands
[2] LaserLaB, Department of Physics and Astronomy, Vrije Universiteit Amsterdam, De Boelelaan 1081, 1081 HV Amsterdam, The Netherlands

[a)] **Author to whom correspondence should be addressed:** l.amitonova@arcnl.nl

ABSTRACT

Light is a perfect tool for numerous metrology applications. To deliver light to hard-to-reach places, fiber probes are widely used. Hair-thin endoscopes based on multimode fibers offer exceptional performance in terms of information density and instrument footprint. Here, we integrate optical metrology into a flexible fiber probe and present a multimode fiber ruler for detecting nanometric displacements. A fast single-shot measurement demonstrates two-dimensional resolving power of 1.8 nm, which is 670 times smaller than the diffraction limit of the optical system and 24 times smaller than the demagnified image pixel size. The multimode fiber ruler does not require detailed field mapping; therefore, low-magnification optical systems can be used to increase the light intensity on a sensor. Moreover, the proposed approach does not rely on any special structures, such as optical grating or metasurfaces. A high-resolution two-dimensional fingerprint is naturally "printed" on the multimode fiber output facet. Our results enable fiber-based displacement measurements with nanometer precision, establishing a new benchmark for fiber-based optical alignment sensors and metrology.

I. INTRODUCTION

Optical imaging has played a central role in numerous research applications from biomedical microscopy[1,2] to semiconductor metrology.[3] High-resolution optical imaging traditionally relies on high-magnification and high-numerical aperture (NA) objectives.[4] In addition to that, methods of nanoscale imaging, such as stimulated emission depletion (STED) microscopy and photoactivated localization microscopy (PALM), require nonlinear interaction with a sample and special fluorescent marks.[5–7]

In many metrology applications, no imaging information is actually required, but displacements, deformations, or overlay should be measured optically with the highest precision.[8] Usually, optical metrology relies on specially designed structures. For example, to allow the position measurement for nanolithography applications, so-called alignment targets are printed in every field on the wafer. Gratings are commonly used as an alignment due to their periodic nature.[9] Therefore, to detect the displacement in two dimensions with gratings, two sets of targets are required. Displacement of the object can be measured optically by using phase singularities of a structured electromagnetic field as marks.[10] Recently, detecting nanometric displacement with Pancharatnam–Berry phase metasurfaces was demonstrated.[11] The approach proposed by Yuan and Zheludev exploits monolithic metamaterial interferometry and can be used for measuring the mutual displacement of two platforms, one with a laser source and a metamaterial mask generating an optical ruler and the other with a magnifying lens, a polarizer, and an image sensor.[11] The transverse displacement of one of the metasurfaces relative to another can be tracked with (sub-)nanometer precision by monitoring the polarization rotation.[12] Nanoscale displacement measurements using integrating sphere concatenated geometry have been demonstrated.[13] These approaches rely on bulky optical components and free-propagation in between.

Compact and flexible multimode (MM) fibers have gained increasing interest in the past decades, emerging as an ultimately thin imaging probe[14–16] as well as a way to boost optical communication networks.[17] Computational methods have been used to push the spatial resolution of MM fiber imaging beyond the diffraction limit.[18] A MM fiber is a perfect tool to perform remote measurements in hard-to-reach places. A speckle pattern caused by the random interference of light propagated via various invariant fiber modes in a MM fiber can act as a fingerprint naturally printed on the fiber output facet.

Speckle metrology spans a rather wide variety of techniques from direct laser speckle photography to speckle interferometry.[19,20] Lateral displacement measurements via MM fiber-based speckle metrology with the resolution in micrometer range has been demonstrated.[21,22] These methods exploit the fact that the speckle pattern on the MM fiber output is largely influenced by the deformations of the fiber caused by its lateral displacement. However, the sensitivity of these techniques was limited by the size of an individual speckle.[23]

Here, we present a MM fiber ruler for detecting nanometric displacements. We use large phase gradients as well as phase singularities of a speckle pattern normally produced by a MM fiber. As illustrated in Fig. 1(a), this natural super-resolved two-dimensional (2D) fingerprint can be exploited in a similar way as a physical ruler. We experimentally demonstrate a displacement resolving power of about 1.8 nm (λ/300, where λ = 532 nm is the wavelength of light) in two dimensions simultaneously by a fast single-shot measurement. It is 670 times smaller than the diffraction limit dictated by the MM fiber. The proposed approach is not limited by NA or magnification of the imaging system. The experimentally demonstrated accuracy is 24 times smaller than the demagnified image pixel size. The sensitivity is limited by only shot noise and thermal and mechanical stabilities of the setup. In contrast to the previous studies, our approach does not require any special structure—optical grating or metasurfaces—to be designed and fabricated. Fiber format opens up numerous application areas in which high resolution and compact size are essential, including lithography mask alignment, precise positioning of components, and monitoring the deformation. Our results enable fiber-based measurements with a nanometer precision via a simple optical setup establishing a new benchmark for fiber-based optical alignment sensors and metrology.

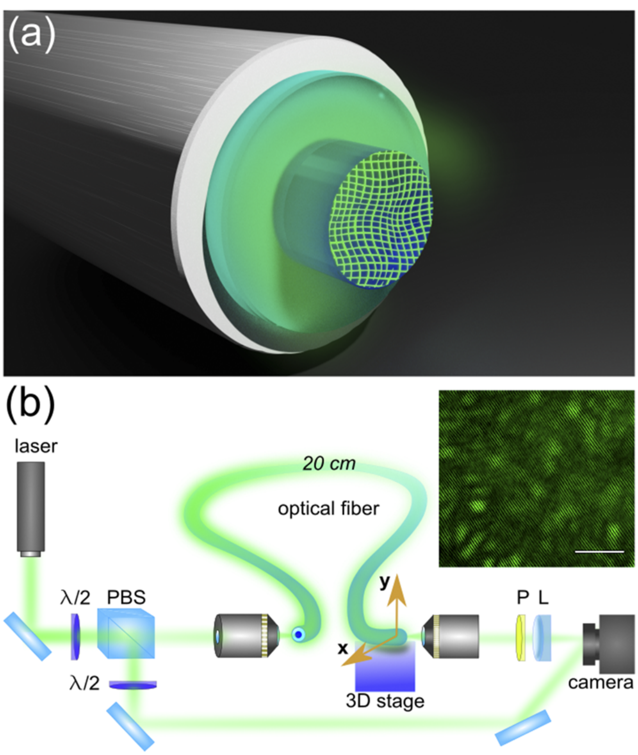

FIG. 1. Principle of nanoscale measurements with fiber-based optical ruler. (a) Artistic illustration of the main concept: The large phase gradients and singularities of a speckle pattern, caused by the random interference of light propagated via various invariant fiber modes, can act as a fingerprint naturally printed on the fiber output facet. (b) Simplified sketch of the experimental setup. The fiber output faced fixed on a nano-positioning piezo stage (3D stage) is imaged on the CCD camera. The off-axis reference beam is used for single-shot holographic phase measurements. PBS, polarizing beam splitter; λ/2, half-wave plate; P, polarizer, L; tube lens. Right: the experimentally measured hologram. The scale bar is 5 μm.

II. RESULTS

The experimental setup is presented in Fig. 1(b). The 2D optical ruler is generated on the output facet of a standard non-connectorized step-index MM fiber (Thorlabs, FG050UGA) with a silica core of 50 μm diameter and a numerical aperture (NA) of 0.22. The length of the fiber is ~20 cm. The fiber has been bent with a single loop, as sketched in Fig. 1(b). For illumination, we use the continuous-wave linearly polarized second-harmonic output of a Nd:YAG laser with a wavelength of 532 nm (Cobolt Samba). The MM fiber supports ~2000 modes at the given wavelength. The laser beam is divided into two pathways by a polarizing beam splitter. The power distribution is controlled by a half-wave plate splitting the light in the reference beam and the signal beam to ensure the best contrast of the hologram. The power of the signal and reference arms is 4 and 10 μW, respectively. The signal beam is coupled to the MM fiber by a 40 (NA = 0.65) microscope objective. Another 40 (NA = 0.75) objective together with a lens (focal length, f = 250 mm) in the 4F configuration is used to image the fiber output facet to the CCD camera (Basler acA3088-57um). The actual magnification factor is measured to be 54, corresponding to the demagnified image pixel size of 44 nm. Therefore, the measured pixel size is significantly larger than the metrology precision we are aiming for. The piezo stage (PI P-616 NanoCube) has been used to control lateral displacement in the y-direction in the metrology experiments. The output facet of the MM fiber has been glued to the fiber holder and fixed on the piezo stage that allows to position the fiber output facet with a nominal resolution of 0.4 nm. The rest of the fiber lies on the optical table with a few fixation points along its length and only about 1 cm of the fiber tip is moved by the stage. The camera and the piezo stage are synchronized and controlled with custom-made software.

The field maps have been recorded by digital off-axis holography.[24] Signals from the MM fiber output and the off-axis reference beam are coherently added on a camera chip forming a hologram. The example is presented in the inset of Fig. 1(b). Two adjustable mirrors in the reference pathway allow for fine-tuning the angle between the signal and reference beams. We set the angle to ensure the spatial separation between the +first- and zero-order terms.

Holographic measurements require a polarized light; therefore, a polarizer and a half-wave plate are used to align polarizations of the two beams interfering on the camera sensor. We apply a 2D Fourier transform to the recorded holographic image and assume an infinite plane wave reference beam. The amplitude of the 2D Fourier transform of the recorded hologram shows three components corresponding to 0, +1, and −1 orders that do not overlap due to the angle between the reference and signal beams. We numerically cut the +1 order in the Fourier domain, move it to the center (zero frequency), and perform the inverse Fourier transform that results in the complex field of the signal beam: amplitude and phase. Therefore, a fast single-shot measurement provides a phase and amplitude image of the fiber output facet.

The zoomed-in images of the reconstructed amplitude and phase are presented in Figs. 2(a) and 2(b), respectively. We see a speckle intensity distribution typical of the MM fiber. Displacement of the fiber can be measured optically with such a system, but the resolution is limited by diffraction. Because of the limited NA, the average size of a speckle is equal to $\lambda/(2\mathrm{NA}) = 1.2\ \mu$m. The individual speckle size, in principle, defines the conventional resolution of such a system.

We estimate the shift by using a correlation between the original pattern and the shifted one. As a result, the characteristic width (the full width of half maximum) of the autocorrelation function gives the estimation of the expected resolution. To quantitatively analyze the potential resolution of speckle-based displacement metrology, we calculate the 2D autocorrelation function of the experimentally measured amplitude speckle map and k-vector map by

$$C(i,j) = \sum_{m,n}^{N} I(m,n)I(m-i,n-j), \tag{1}$$

where I is the pixilated $N \times N$ matrix of the intensity distribution and i, j, m, n are indices of the image pixels. The results are presented in Fig. 2(d) by a cross section along the x axis while $y = 0$. We see that the full width of the central peak, which is responsible for speckle decorrelation, is about 1.2 μm, as expected.

In the next step, we follow the idea recently proposed by Yuan and Zheludev[11] and calculate the modulus of the local wave vector $k = \Delta\varphi$, where φ is the phase distribution presented in Fig. 2(b). The resulting local wave vector map demonstrates peaks that are significantly narrower than the intensity hotspot (speckles) itself as presented in Fig. 2(c). The white lines correspond to the artificial phase jump from $-\pi$ to π, while the red endpoints of the lines represent the phase singularities. While the phase singularities are the areas of physically rapidly changing phase, the phase jumps from $-\pi$ to π are the results of the mathematical definition of the

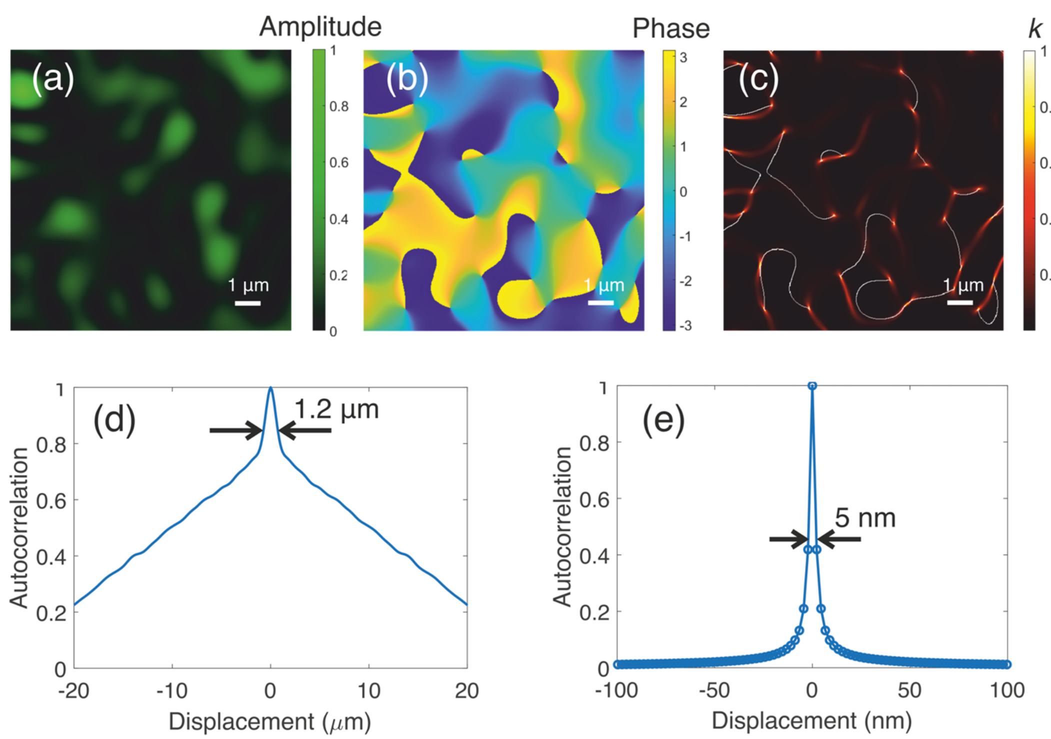

FIG. 2. Experimental demonstration of fiber-based displacement measurements. (a) Zoomed-in amplitude (A) (a) and phase (φ) (b) on the output facet of the MM fiber experimentally measured by off-axis holography. (c) Modulus of the local wave vector $k = \Delta\varphi$ on the MM fiber output. The areas of rapid variations of phase (peaks of k) are much narrower than the speckle size. Scale bars are 1 μm. Cross sections along the x axis while $y = 0$ of the autocorrelation functions calculated for the experimentally measured amplitude speckle map (d) and modulus of the local wave vector k (e).

phase and are not related to any physical phenomenon. We removed the artificial phase jumps, leaving only phase singularities for further processing. We can use these lines naturally projected on the MM fiber output as "ticks" of the 2D optical ruler for the precise displacement measurements.

Because of the relatively low magnification of our imaging system, the effective pixel size, which is 44 nm, may limit our accuracy. However, the proposed approach allows us to numerically make the pixel size infinitely small by zero-padding.[25] The total number of pixels can be augmented by padding the matrix of the hologram with zeros in both the horizontal and vertical directions. Zero-padding helps us to decrease the pixel size more than ten times. Without the zero-padding procedure, we would be limited by the effective image pixel size. In our experiments, we analyze the central area of the fiber facet with the size of $28.35 \times 28.35\ \mu\mathrm{m}^2$. By zero-padding in the Fourier domain, we increase the total number of pixels from 644×644 to $12\,800 \times 12\,800$, making an effective pixel size of only 2.2 nm.

We estimate the potential metrology resolution by the autocorrelated function calculated for the wave vector map k. The results are presented in Fig. 2(e) by a cross section along the x axis while y is 0. We see that the autocorrelation function decays rapidly, providing an expected resolution of about 5 nm. As a result, a much better resolving power can be achieved by using a k-vector map instead of a speckle pattern amplitude.

To evaluate the practically achievable resolution of the MM fiber optical ruler, we perform a displacement metrology experiment. We move the fiber output facet in the vertical y-direction by the piezo stage. Only the fiber output is fixed on the movable stage and all other components of the setup remain stable. The fiber has been displaced by 100 nm in 20 nm steps. For each position, a single camera image with an exposure time of 1.4 ms is recorded. The fiber displacement is extracted by calculating the 2D cross-correlation function between the two k-vector maps: one that corresponds to the original (zero) position and another that corresponds to the shifted position of the fiber facet. The coordinates of a maximum value of the 2D cross-correlation provide the measured shift. The proposed approach is inherently two-dimensional because of the 2D structure of the k-vector map presented in Fig. 2(c).

The experiment was repeated five times. The results are presented in Fig. 3, where the blue circles represent the measured shift in the vertical direction as a function of the displacement controlled by the piezo stage. The red circles represent the measured shift in the horizontal direction. Error bars show the standard deviation. Dashed lines indicate the expected shift in both horizontal (x-) and vertical (y-)directions. The standard deviation for all the measurements is 1.2 nm. We estimate the accuracy of our approach by calculating root-mean-square deviation (RMSD) between the experimentally measured values and the set values of the nano-positioning stage as

$$\mathrm{RMSD} = \sum \sqrt{\frac{(y_{0m} - y_m)^2}{N}}, \tag{2}$$

where N is the total number of measurements.

Our experiments demonstrate an accuracy of 1.8 nm over a displacement range of 100 nm, as presented in Fig. 3. It can be seen that at large distances, the measured shift starts to deviate from the set values. One of the reasons could be that the vertical direction in the experiment is not exactly aligned with the vertical direction in the processing. Another possible explanation is that at about 100 nm, shift speckle patterns start to deviate enough to degrade the displacement measurements. The model proposed by Plöschner *et al.*[26] could be further used to calculate changes in the speckle pattern and to improve metrology accuracy further. The calculated RMSD determines the displacement resolving power of the optical ruler to be 670 times better than the diffraction limit dictated by the limited NA of the MM fiber and 300 times smaller than the wavelength of light.

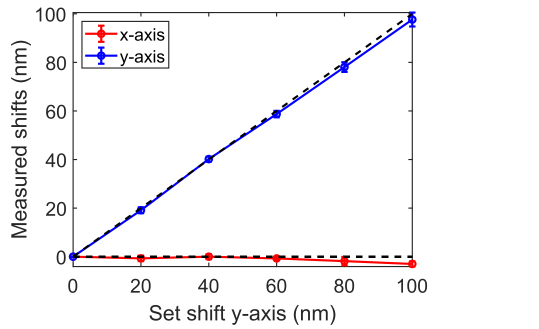

FIG. 3. Experimentally measured shift of the MM fiber facet as a function of the displacement set by the piezo stage. The blue and red circles represent the shift averaged over five measurements in the vertical and horizontal directions, respectively, and error bars show the standard deviation. Dashed lines indicate the expected shift in both directions.

To evaluate the theoretically achievable metrology resolution, we performed numerical experiments. Experimentally measured field on the fiber output $E_0(x,y)$ was normalized and re-scaled to high number of pixels, digitally shifted to the certain distance (from 0 to 15 nm) along both x and y axes, and scaled back to the original 1400×1400 pixel camera image creating shifted field $E_{shift}(x,y)$. Intensities of the each pixel of $E_{shift}(x,y)$ were scaled in such a way as to represent the number of "detected" photons N_p. We added shot noise to the field by generating random numbers from the Poisson distribution specified by the number of photons and used the generated numbers instead of original intensities for further processing. We simulated the digital holography experiment by numerically adding a reference plane wave E_{ref} at an angle to the signal beam.

The hologram has been processed in the same way as in the actual experiments and the shifts in x- and y-directions were extracted from the k-vector map. We repeat simulations for different displacements and different number of photons in the signal beam. The results for $N_p = 10^{10}$, 10^9, and $2 \cdot 10^8$ are presented in Fig. 4(a) by circles, squares, and triangles, respectively. Shift in the vertical and horizontal directions is shown by blue and red colors, respectively. The dashed lines represent the ground truth.

We analyzed the results using RMSD as described before [Eq. (2)]. The results are presented in Fig. 4(b). In theory with more than 10^{10} photons (which is about 5 nW), 1 nm displacement can measured with 0.1 nm accuracy. A total of 10^9 photons (which corresponds to only 500 photons per camera pixel on average) allow us to reach sub-nm precision (RMSD = 0.5 nm). We repeated the

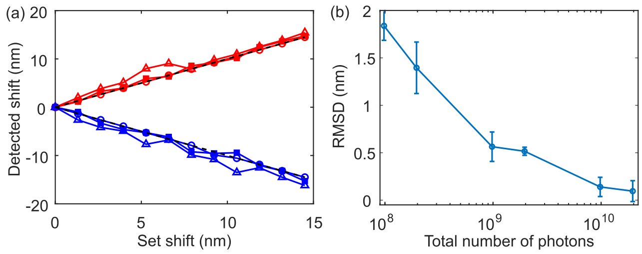

FIG. 4. Results of numerical experiments. (a) The displacement of MM fiber facet along the *x* axis (red) and *y* axis (blue) as a function of the ground truth for different incident number of photons: 10^{10} (circles), 10^9 (squares), and $2 \cdot 10^8$ (triangles). Dashed lines indicate the ground truth. (b) Root-mean-square deviation (RMSD) as a function of the total number of photons. Circles represent the average value and error bars show the standard deviation.

simulations with $N_p = 10^{10}$ photons and applied the same analysis directly to the speckle intensity and speckle field distributions, which resulted in RMSD of 92 and 71 nm, respectively. Analytical approximations[27] or complex wavefront shaping[28] can be used to further improve position detection accuracy for both *k*-vector and intensity-based approaches.

III. CONCLUSION AND DISCUSSION

In this study, we experimentally demonstrated the MM fiber optical ruler for displacement or alignment metrology with nanometric precision. In our experiments, 2D displacement resolving power of about 1.8 nm by a fast (1.4 ms) single-shot measurement has been demonstrated. The actual measurement speed was limited by our camera frame rate, which is 69 fps. The experimentally demonstrated accuracy is 670 times smaller than the diffraction limit dictated by the MM fiber and 300 times smaller than the wavelength of the light. The proposed approach does not require detailed field mapping and, therefore, is not limited by the NA, magnification of the imaging system, and the original image pixel size. Therefore, low-magnification optical systems and camera sensors with a relatively low number of pixels can be used. It helps to increase the light intensity on the sensor in the case of a low photon budget and, therefore, to decrease shot noise.

The noiseless amplification[29] allows for overcoming thermal and read-out noise of the detector. As a result, the sensitivity is limited by the shot noise as well as by mechanical and thermal instabilities of the elements. Our simulations predict higher accuracy for the given number of photons and ideal conditions, indicating that the experiments were environmental stability limited. Moreover, the displacement of the output fiber facet changes the light propagation via the MM fiber and the interference pattern on the fiber output[30] and can be a limiting factor for the maximum detection range. Despite the common way of seeing MM fibers as unpredictable optical systems, the link between the input and output fields can be expressed as a linear transformation.[31] Plöschner *et al.* proposed a theoretical model to predict light propagation within significantly deformed segments of multimode fibers.[26] A similar approach could be applied to other environmental distortions. Reducing the multimode fiber length also helps to minimize the undesired effects. The stability of the MM fiber-based ruler can be improved without sacrificing its length by splicing a long single-mode fiber with a relatively short piece of a multimode fiber. The single-mode part would ensure that the light is delivered without perturbations and the multimode part can be used as a sensor. Another way to increase displacement accuracy is to use a fiber with a larger core diameter and, consequently, a higher number of "ticks."

In contrast to the previous works, our approach does not require any special structures—optical grating or metasurfaces—to be designed and fabricated. Fiber format opens up numerous application areas in which high resolution and compact size are essential, including stage calibration, x-ray mirror metrology,[32] and in-operando and *in situ* monitoring of stress evolution in electrodes of Li-ion batteries.[33] The fiber ruler can be implemented in either transmission geometry where the fiber is mounted on the object under test or reflection geometry where the fiber illuminates the surface. In the future, the proposed approach can be applied to the in-other-way-inaccessible environment by using a multimode fiber as an optical ruler and a multicore fiber probe to record a shifted speckle pattern and to deliver it to the detector. We demonstrated that the resolution of our approach does not really depend on a camera pixel size (which was more than 20 times bigger than the final resolution). Therefore, a flexible multi single-core probe can be used to deliver an image.[34,35] The demonstrated MM fiber ruler paves new ways toward ultimately compact fiber-based optical metrology sensors.

ACKNOWLEDGMENTS

We thank Gerwin Osnabrugge (ARCNL) for fruitful discussions and Marco Seynen (AMOLF) for data acquisition software. This work was carried out within the ARCNL, a public–private partnership between UvA, VU, NWO, and ASML, and was partly financed by "Toeslag voor Topconsortia voor Kennis en Innovatie (TKI)" from the Dutch Ministry of Economic Affairs and Climate Policy.

AUTHOR DECLARATIONS

Conflict of Interest

The authors have no conflicts to disclose.

Author Contributions

Ksenia Abrashitova: Formal analysis (equal); Investigation (equal); Methodology (equal); Writing – original draft (equal); Writing – review & editing (equal). **Lyubov V. Amitonova:** Conceptualization (lead); Formal analysis (equal); Investigation (equal); Methodology (equal); Supervision (lead); Writing – original draft (equal); Writing – review & editing (equal).

DATA AVAILABILITY

The data that support the findings of this study are available from the corresponding author upon reasonable request.

REFERENCES

[1] S. Yoon, M. Kim, M. Jang, Y. Choi, W. Choi, S. Kang, and W. Choi, "Deep optical imaging within complex scattering media," Nat. Rev. Phys. **2**, 141–158 (2020).

[2] V. Ntziachristos, "Going deeper than microscopy: The optical imaging Frontier in biology," Nat. Methods **7**, 603–614 (2010).

[3] W. Osten and N. Reingand, *Optical Imaging and Metrology: Advanced Technologies* (John Wiley & Sons, 2012).

[4] J. Mertz, *Introduction to Optical Microscopy* (Cambridge University Press, 2019).

[5] S. W. Hell, "Far-field optical nanoscopy," Science **316**, 1153–1158 (2007).

[6] S. W. Hell, "Microscopy and its focal switch," Nat. Methods **6**, 24–32 (2009).

[7] L. Schermelleh, A. Ferrand, T. Huser, C. Eggeling, M. Sauer, O. Biehlmaier, and G. P. C. Drummen, "Super-resolution microscopy demystified," Nat. Cell Biol. **21**, 72–84 (2019).

[8] D. Bouchet, S. Rotter, and A. P. Mosk, "Maximum information states for coherent scattering measurements," Nat. Phys. **17**, 564–568 (2021).

[9] A. J. den Boef, "Optical wafer metrology sensors for process-robust cd and overlay control in semiconductor device manufacturing," Surf. Topogr.: Metrol. Prop. **4**, 023001 (2016).

[10] N. I. Zheludev and G. Yuan, "Optical superoscillation technologies beyond the diffraction limit," Nat. Rev. Phys. **4**, 16 (2021).

[11] G. H. Yuan and N. I. Zheludev, "Detecting nanometric displacements with optical ruler metrology," Science **364**, 771–775 (2019).

[12] R. Barboza, A. Babazadeh, L. Marrucci, F. Cardano, C. de Lisio, and V. D'Ambrosio, "Ultra-sensitive measurement of transverse displacements with linear photonic gears," Nat. Commun. **13**, 1080 (2022).

[13] M. Facchin, G. D. Bruce, and K. Dholakia, "Measuring picometre-level displacements using speckle patterns produced by an integrating sphere," arXiv:2110.15939 (2021).

[14] R. Di Leonardo and S. Bianchi, "Hologram transmission through multi-mode optical fibers," Opt. Express **19**, 247–254 (2011).

[15] T. Čižmár and K. Dholakia, "Shaping the light transmission through a multimode optical fibre: Complex transformation analysis and applications in biophotonics," Opt. Express **19**, 18871–18884 (2011).

[16] D. Stellinga, D. B. Phillips, S. P. Mekhail, A. Selyem, S. Turtaev, T. Čižmár, and M. J. Padgett, "Time-of-flight 3D imaging through multimode optical fibers," Science **374**, 1395–1399 (2021).

[17] L. V. Amitonova, T. B. H. Tentrup, I. M. Vellekoop, and P. W. H. Pinkse, "Quantum key establishment via a multimode fiber," Opt. Express **28**, 5965–5981 (2020).

[18] L. V. Amitonova and J. F. de Boer, "Endo-microscopy beyond the Abbe and Nyquist limits," Light: Sci. Appl. **9**, 81 (2020).

[19] J. A. Leendertz, "Interferometric displacement measurement on scattering surfaces utilizing speckle effect," J. Phys. E: Sci. Instrum. **3**, 214 (1970).

[20] E. Archbold, J. M. Burch, and A. E. Ennos, "Recording of in-plane surface displacement by double-exposure speckle photography," Opt. Acta **17**, 883–898 (1970).

[21] F. T. S. Yu, M. Wen, S. Yin, and C.-M. Uang, "Submicrometer displacement sensing using inner-product multimode fiber speckle fields," Appl. Opt. **32**, 4685–4689 (1993).

[22] Y. Liu, Q. Qin, H.-h. Liu, Z.-w. Tan, and M.-g. Wang, "Investigation of an image processing method of step-index multimode fiber specklegram and its application on lateral displacement sensing," Opt. Fiber Technol. **46**, 48–53 (2018).

[23] J. W. Goodman, *Speckle Phenomena in Optics: Theory and Applications* (Roberts and Company Publishers, 2007).

[24] E. Cuche, P. Marquet, and C. Depeursinge, "Simultaneous amplitude-contrast and quantitative phase-contrast microscopy by numerical reconstruction of Fresnel off-axis holograms," Appl. Opt. **38**, 6994–7001 (1999).

[25] P. Ferraro, S. De Nicola, G. Coppola, A. Finizio, D. Alfieri, and G. Pierattini, "Controlling image size as a function of distance and wavelength in Fresnel-transform reconstruction of digital holograms," Opt. Lett. **29**, 854–856 (2004).

[26] M. Plöschner, T. Tyc, and T. Čižmár, "Seeing through chaos in multimode fibres," Nat. Photonics **9**, 529–535 (2015).

[27] S. Wolter, M. Schüttpelz, M. Tscherepanow, S. van de Linde, M. Heilemann, and M. Sauer, "Real-time computation of subdiffraction-resolution fluorescence images," J. Microsc. **237**, 12–22 (2010).

[28] E. G. van Putten, A. Lagendijk, and A. P. Mosk, "Nonimaging speckle interferometry for high-speed nanometer-scale position detection," Opt. Lett. **37**, 1070–1072 (2012).

[29] F. Charrière, T. Colomb, F. Montfort, E. Cuche, P. Marquet, and C. Depeursinge, "Shot-noise influence on the reconstructed phase image signal-to-noise ratio in digital holographic microscopy," Appl. Opt. **45**, 7667–7673 (2006).

[30] G. Li, Y. Liu, Q. Qin, X. Zou, M. Wang, and F. Yan, "Deep learning based optical curvature sensor through specklegram detection of multimode fiber," Opt. Laser Technol. **149**, 107873 (2022).

[31] A. W. Snyder and J. Love, *Optical Waveguide Theory* (Springer Science & Business Media, 2012).

[32] H. Wang, S. Moriconi, and K. Sawhney, "Nano-precision metrology of X-ray mirrors with laser speckle angular measurement," Light: Sci. Appl. **10**, 195 (2021).

[33] J. Chen, A. K. Thapa, and T. A. Berfield, "*In-situ* characterization of strain in lithium battery working electrodes," J. Power Sources **271**, 406–413 (2014).

[34] V. Tsvirkun, S. Sivankutty, G. Bouwmans, O. Katz, E. R. Andresen, and H. Rigneault, "Widefield lensless endoscopy with a multicore fiber," Opt. Lett. **41**, 4771–4774 (2016).

[35] O. Coquoz, R. Conde, F. Taleblou, and C. Depeursinge, "Performances of endoscopic holography with a multicore optical fiber," Appl. Opt. **34**, 7186–7193 (1995).